PROCEEDINGS, 43rd Workshop on Geothermal Reservoir Engineering
Stanford University, Stanford, California, February 12-14, 2018
SGP-TR-213

Review of the Hawaii Play Fairway Phase 2 Activities

Nicole Lautze, Donald Thomas, Garrett Ito, Neil Frazer, Stephen Martel, Nicholas Hinz, Robert Whittier

1680 East West Address Road, POST 602 Honolulu, HI 96822

lautze@hawaii.edu

Keywords: Hawaii, volcano, groundwater, geophysics, magnetotelluric, stess, model

ABSTRACT

The Hawaii Play Fairway project, funded by the U.S. Department of Energy, comprises three Phases. In Phase 1, existing geologic, groundwater, and geophysical datasets relevant to subsurface heat, fluid and permeability were identified, compiled, and ranked. We also developed a statistical methodology to integrate these data into a resource probability map. Phase 2 of the project has involved the collection of new groundwater data in ten prospective regions across the state; collection of new geophysical data on Lanai, Maui, and central Hawaii Island; and modeling of topographically induced stresses - the last to better characterize permeability. Phase 2 data were incorporated into an updated resource probability map. Here, we present results of the Phase 2 data collection and modeling activities, and comment on Phase 3 plans.

1. INTRODUCTION

Electricity prices in the State of Hawaii are the highest in the US and about double the national average, in part because roughly 80% of Hawaii's energy is from imported petroleum. The Hawaiian Islands are volcanic in origin, yet the extent of the State of Hawaii's geothermal resource is largely uncharacterized. A statewide geothermal resource assessment published in 1985 found a potential resource on all islands. Since that date, little additional exploration was undertaken, until this Play Fairway project. The project has been a major step forward for the State of Hawaii, providing an updated resource assessment, a roadmap for additional exploration activities, and identification of target sites for drilling.

In Phase 1, the Hawaii Play Fairway team developed a broadly applicable method for integrated data analysis using a Bayesian statistical approach, produced a ranked evaluation of geothermal resources for Hawaii, and defined a roadmap for site-specific exploration activities based on maps of calculated resource probability, confidence in those maps, and an assessment of the viability of development. These activities and results are detailed in Lautze et al., (2017a;b) and Ito et al. (2017).

For Phase 2, the team defined four sets of activities, each of which was successfully completed (Table 1).

1) *Collect groundwater samples* in 10 areas of interest across the state and analyze for a) consistency with legacy data compiled in Phase 1, b) geothermal indicators, and c) the refinement of inferred groundwater flow direction. Broadly speaking, Phase 2 groundwater data reinforce the Phase 1 legacy data. Phase 2 data confirm the presence of multiple warm water wells on the east coast of Kauai, in Waianae's caldera region (Oahu), Lanai's caldera region, and along the Northwest and Southern coasts of Hawaii Island. Geochemical data lend further evidence for the presence of high crustal temperatures in some of these areas. Isotopic data were used to improve upon modeled groundwater flow trajectories on Lanai.

2) *Produce 3D models of crustal stress due to topography* to inform the probability of fracture-induced permeability. We developed a first-order method for computing topographic stresses using Green's functions that is more than an order of magnitude faster than existing boundary element or finite element numerical methods. The new results, as well as our ongoing and prior research indicate that topography can induce appreciable crustal stresses, and in places, can enhance permeability through fracturing.

3) *Perform MT and gravity surveys and geophysical inversions in three target areas: Lanai Island, Mauna Kea, and Haleakala Volcano's SW Rift Zone (Maui)*. The augmented gravity and new MT data sets were inverted to solve for subsurface density and resistivity structure, respectively. The results provide a basis for evaluating potential drilling targets and depths and for establishing conceptual models about hydrologic and geothermal processes.

4) *Produce updated resource probability maps and confidence in those maps.* We developed a method to incorporate depth information about resistivity, density, and topographic stresses into our voter-veto method of computing the relative probabilities of heat, fluid, permeability and a viable resource, as well as confidence in those probabilities. New maps of probability and confidence were made for the whole state, as well as for the three targeted geophysical survey areas.

TABLE 1.

PHASE2 OBJECTIVE	OUTPUT	OUTCOME
Groundwater Sampling	• 62 samples collected in 10 areas • analyzed for temperature, major elements, trace elements and isotopes	• Validated PHASE1 legacy data • Anomalies identified on 3 islands
Topographic Stress Modeling	3D models of stresses for all target islands	Added information to inform the probability of permeability at depth and increased confidence.
Geophysical Surveys	• Collected new data from 44 MT sites on Lanai, 8 on Maui. • New inversions of 4 (pre-existing) MT transects around Mauna Kea • Collected new gravity data on Lanai (140 pts) and east and SE of Mauna Kea (73 pts) • Acquired and inverted a dense gravity survey of Haleakala's SE Rift Zone done by ORMAT	Models of depth-varying resistivity and density structure allow us to reject some areas and accept others for potential geothermal reservoirs.
New calculations of probability and confidence	Updated maps of probability of heat, permeability, fluid, and geothermal resources across Hawaii and in the 3 geophysical survey areas	• Improved assessment of resource potential statewide. • New probability and confidence maps of geophysical survey areas inform where and where not to drill.
Rank Drilling Plays for PHASE3	Qualitative and quantitative evaluations of all data in the 3 geophysical survey areas	

2. METHODS AND RESULTS

2.1 Groundwater Campaign

Groundwater samples were collected in the 10 locations of Phase 2 focus areas at the conclusion of Phase 1 (red boxes, Fig 1, 2). A total of 61 samples were collected from existing wells, and one spring was sampled in an area where no wells exist (SE of Mauna Kea). Standard field methods were followed. Parameters including groundwater temperature, pH, dissolved oxygen and specific conductivity were measured in the field using a YSI Pro Plus Meter. Groundwater samples collected in the field were distributed among three laboratories at the University of Hawaii at Manoa: the Water Resources Research Center (WRRC) Chemistry Laboratory analyzed for major ions using an ion chromatograph via the EPA method [*Pfaff*, 1993; *Hautman et al.*, 1997]. The Inductively Coupled Plasma (ICP) Facility analyzed for trace metals and silica using a Varian Vista MPX ICP optical emission spectrometer following standard methods [*Martin et al.*, 1992]. The Biogeochemical Stable Isotope Facility analyzed for oxygen, deuterium, and carbon-13 isotopes. The 13C isotopes were measured using an automated headspace sampling and continuous-flow mass spectrometry [*Torres et al.*, 2005]. The ^{18}O and D isotopes are measured using a Picarro cavity ring down spectrometer [*Godoy et al.,* 2012].

Key results are shown in **Figs. 1 and 2**. We note a general consistency between Phase1 legacy and Phase 2 data. Anomalously warm wells were identified along the NW coast, South point and the Puna region of Hawaii Island, along the SW rift zone of Haleakala (Maui), in multiple wells central to Lanai, and in the Waianae caldera region (SW Oahu). In general, geochemistry patterns are consistent with the thermal anomalies. The isotope data were used to improve groundwater flow paths, with a focus on Lanai. Not enough wells (Phase 2 data points) exist to use this technique in many locations across the state.

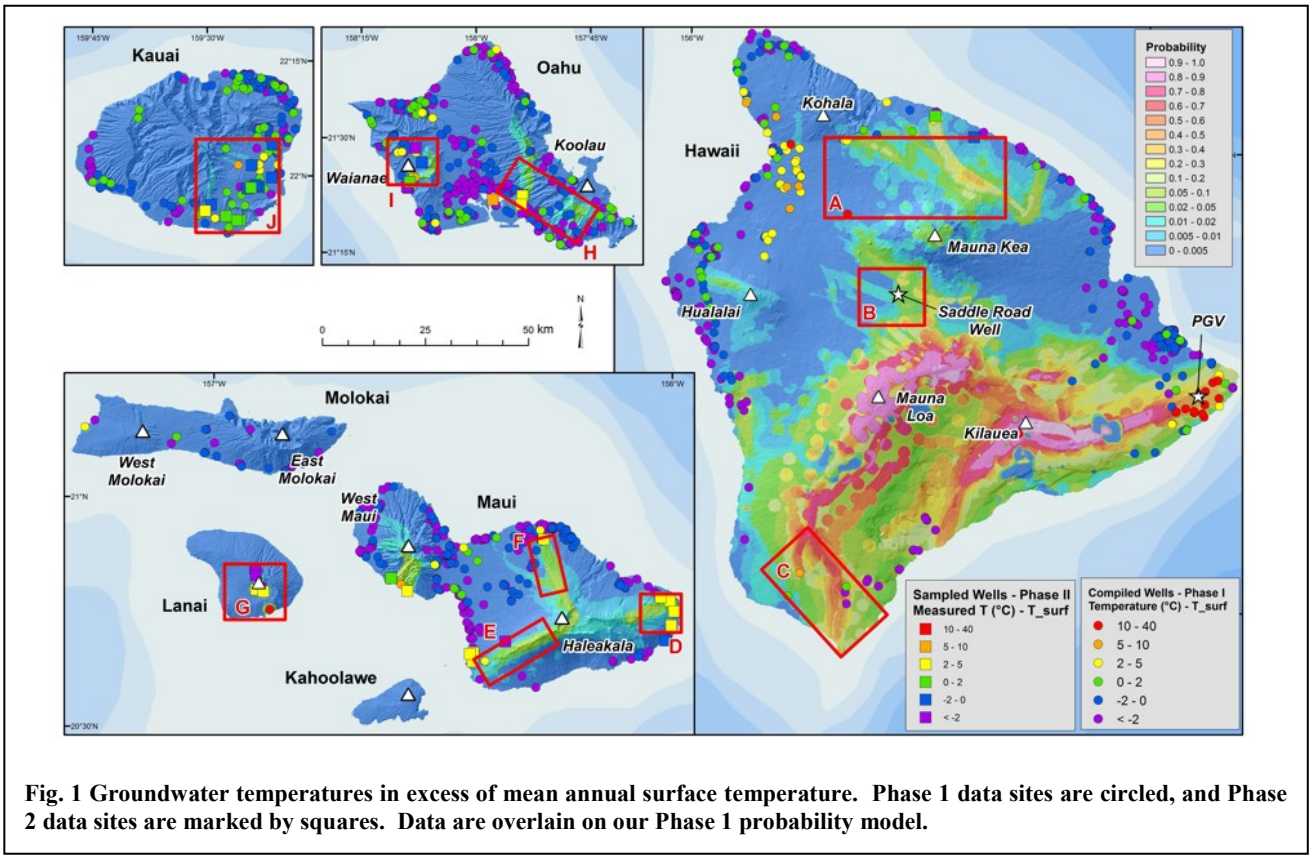

Fig. 1 Groundwater temperatures in excess of mean annual surface temperature. Phase 1 data sites are circled, and Phase 2 data sites are marked by squares. Data are overlain on our Phase 1 probability model.

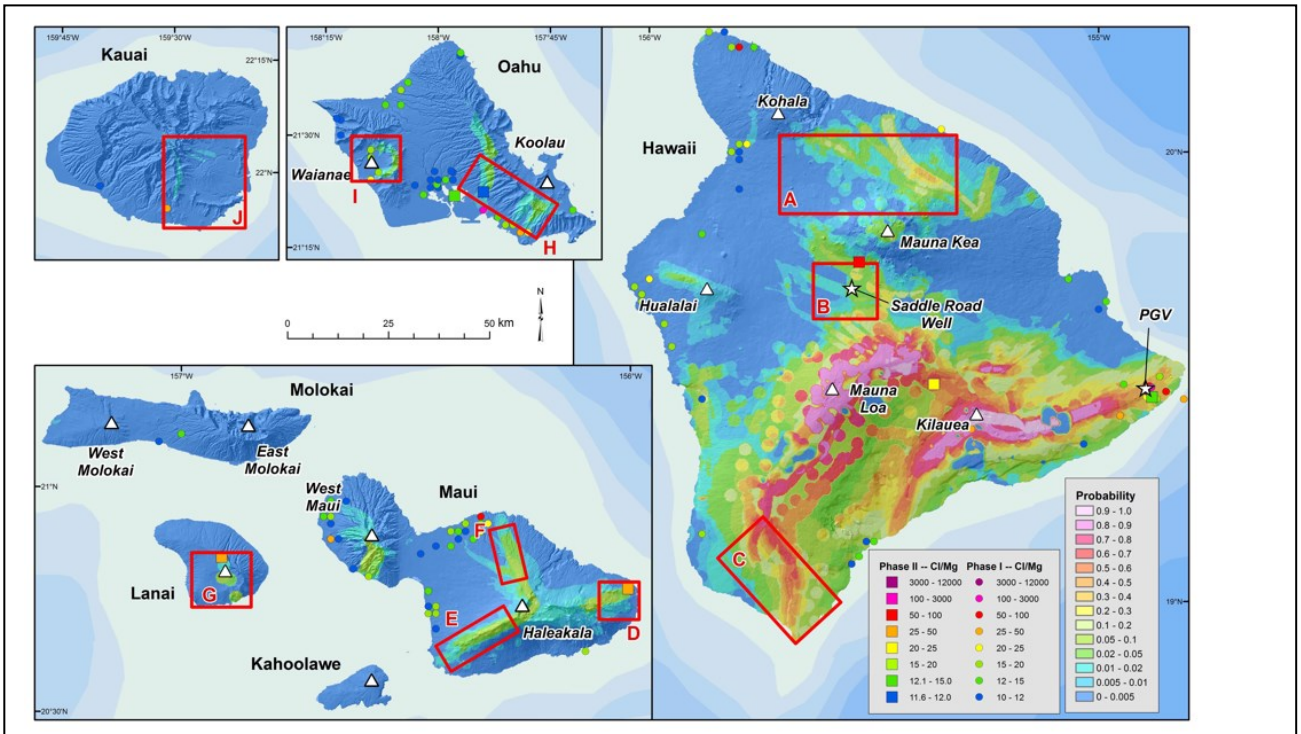

Fig. 2. Map of only the Cl/Mg ratios that are considered anomalous. Phase 1 data sites are circled, and Phase 2 data sites are marked by squares. Data are superimposed on our Phase 1 probability model.

2.2 Topographic Stresses and Failure Potential

We use a forward modeling method to calculate the stresses due to gravity within the Hawaiian volcanoes. The method assumes that the total stress (σ^{total}) at a point is the sum of an ambient stress $(\sigma^{ambient})$, independent of topography that arises from a gravitational body force, and a stress perturbation ($\Delta\sigma^{topography}$) due to topography:

$$\sigma^{total} = \sigma^{ambient} + \Delta\sigma^{topography} \quad (1)$$

The topographic stress perturbation is evaluated using a modified version of the solution for a normal traction perturbation acting over a rectangular patch on the surface of an elastic half-space (Love, 1929). The original solution of Love (1929) yields stresses below a datum plane; the modification allows the solution to be extended to *above* the datum plane. The modified solution can then approximate stresses below the topographic surface no matter whether it lies above or below the datum plane. Provided that the amplitude of the topography is small relative to the wavelength of the topography, the traction perturbation applied to the horizontal surface of the half-space closely approximates the traction experienced on a gently sloping topographic surface. If the ambient stress and traction perturbations are properly selected, then their sum yields a total stress along the topographic surface that is compatible with the desired boundary conditions there. For the subaerial portion of a volcano, the desired total traction on the topographic surface equals zero. For the submarine portion of a volcano, the desired total traction equals the water pressure.

The effects of a series of patch perturbation tractions are summed to give the total perturbation due to three-dimensional topography of arbitrary shape, and then added to the ambient stress to give the total stress at any point (**Fig. 3**). The total solution closely approximates the exact total elastic solution. This forward solution method is much faster than techniques that rely on inverse methods.

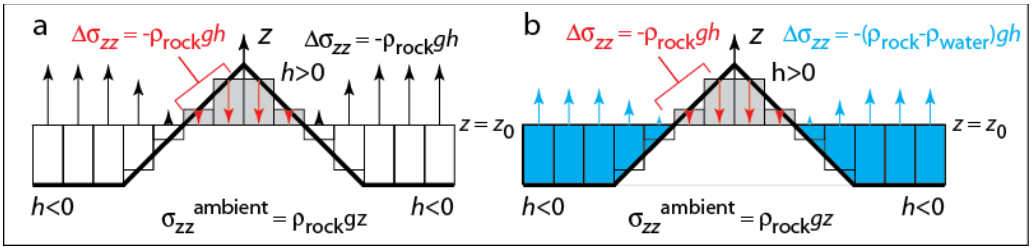

Fig. 3 Ambient stress field and topographic perturbation for two models of a volcano. The datum plane is at elevation z_0. The z-axis points up. The other vertical arrows that extend up from the datum plane, or down to it, indicate topographic traction perturbations. The rectangles represent the discretization of topography where volcanic mass is present above the datum plane (gray) or absent below it (white). (a) The traction acting on the topographic surface of a subaerial volcano (bold) equals zero everywhere. (b) Ambient stress field and topographic perturbation for a model of a volcano built upon the sea floor, with water shown in blue. The total traction acting on the topographic surface of the model volcano equals zero for the subaerial surface, but equals the water pressure along the submarine portion of the surface.

The ambient stress field due to gravity for topography with gentle slopes is dominated by the vertical stress, $\sigma_{zz}^{ambient} = \rho_{rock} g z$, where ρ_{rock} is the rock density (2700 kg/m^3), g is gravitational acceleration, and the vertical z-axis points up. Compressive stresses are considered to be negative. We chose the datum plane elevation (z_0) as sea level, so $z_0 = 0$. The magnitude of the perturbation traction applied to the datum plane is set to $-\rho_{rock} gh$ and to $-(\rho_{rock} - \rho_{water})gh$ for subaerial and submarine portions of a volcano, respectively, where h is the height of the surface of the volcano above the datum plane. For subaerial topography, $h > 0$ and the traction perturbation acts down; for submarine topography, $h < 0$ and the traction perturbation is up.

Failure potential (ϕ) [*Martel* 2000, 2016] serves as a measure of shear fracture susceptibility,

$$\phi = \left| \frac{(\sigma_1 - \sigma_3)}{(\sigma_1 + \sigma_3)} \right| , \quad (2)$$

where σ_1 and σ_3 are the most tensile (least compressive) and least tensile (most compressive) principal stresses, respectively. The numerator is the differential stress, twice the maximum shear stress. The denominator is about twice the mean normal stress. Where the differential stress is small relative to the mean normal stress (i.e., $\sigma_1 \approx \sigma_3$) , ϕ is near zero. Where the differential stress is large relative to the mean normal stress, ϕ is large. As ϕ increases, the stress state favors shearing along fractures and the opening of fractures near the tips of sheared fractures. We consider the failure potential as a proxy for fracture permeability (**Fig 4.** shows results for Lanai Island as an example).

2.3 Gravity Data

Gravity surveys were completed for the island of Lanai and the east flank of Mauna Kea volcano on Hawaii Island to prospect for dense intrusions, which are the source rocks for geothermal heat in Hawaii. We also have used the closely-spaced gravity survey data from Haleakala's southwest rift zone provided by Ormat. The raw data were first corrected for instrument drift and then converted to absolute gravity using ties to an absolute measurement established by the NGIA in 2015 on the Univ. of Hawaii, Manoa campus. Complete Bouguer anomalies Δg_B were then computed by removing the gravity appropriate for the WGS84 reference ellipsoid, and correcting for elevation (free-air correction) as well as the mass of rock associated with topography using a reference density of ρ_0 (Bouguer correction). The anomaly Δg_B reflects density deviations from the reference structure, which includes deviations at both the regional (of orders larger than a few tens of km and greater) and local (tens of km and less) scales. Our focus is the local scale; therefore we subtracted a reference value Δg_{B0} representing the regional contribution. This produces the *local* complete Bouguer anomaly $\Delta g_{BL} = \Delta g_B - \Delta g_{B0}$.

The local anomaly Δg_{BL} was then inverted to produce solutions for 3D density structure. The inversion software, GRAV3D [*GRAV3D*, 2015], is a well-established industry standard that provides the versatility and efficiency needed for our application. We used it to solve for structure that deviates from a reference density structure—here uniform and equal to ρ_0—by a minimal amount needed to fit the data to within a specified tolerance. The tolerance was defined such that the square misfits to the data, normalized by the standard error of the measurements, has a mean of 1 (i.e., the chi-squared misfit equals the number of measurements). In other words, the inversions produced the smoothest solutions that fit the data, and every solution fits the data equally well.

As solutions to gravity inversions are inherently non-unique, the range of plausible solutions must be guided by prior information about the local geology. A variable to which the final results are highly sensitive is the density ρ_0 used for the Bouguer correction and is the reference density used by the inversions. From densities measured along the Hawaiian Scientific Drilling Program (HSDP), which penetrated ~3 km into Mauna Kea's crust [*Moore* 2001], we define a prior probability density function (pdf) for ρ_0. Solutions for crustal density were found using a Monte Carlo sampling method: we repeatedly sampled from the prior pdf for ρ_0, computed the local complete Bouguer anomaly, and inverted for the structure many (10^3) times. The thousand solutions were then used to compute various statistics at each point of the 3D model to assess the most probable locations of the dense intrusive source rock (**Fig. 5**).

2.4 Magnetotellurics

The University of Hawaii's (seven) Phoenix Geophysics MTU-5A receivers and magnetic coil and electrode sets were used to collect 44 MT sites on Lanai and 8 MT sites on Haleakala's SW rift (Maui) using PHASE2 funding. Via outside funding, additional MT data were collected at four new MT sites N of Mauna Kea, and at two sites SE of Mauna Kea, to supplement data already collected in these areas. All new data collected were incorporated into our PHASE2 probability and confidence results.

Data were collected using standard field methods. After a site was selected and the sensors installed, the MTU-5A receiver was programmed to immediately begin recording. Eighteen hours is the minimum amount of time required to collect 10,000 second data. All the sites that were processed had at least 24 hours worth of data for remote and rover receivers. These data, the time series (TS), are collected on compact flash (CF) cards. After the three-day recording session the CF cards were retrieved and the TS are imported into SSMT-2000 - a Phoenix Geophysics program that can process and help evaluate the TS data. The time series were inspected and Discrete Fourier transforms created. The Fourier transforms were then converted into cross-powers using a robust processing routine that uses remote MT site data to reduce noise from the soundings. Data can then be displayed graphically and the cross-powers edited before being converted into Electronic Digital Interchange (EDI) industry-standard files. EDI files for each site were then imported into interpretation software, such as WinGlink, for further processing.

EDI files were added to the Maui and Big Island MT databases in WinGlink. The locations were verified and correctly placed in space. The station data were smoothed using D+ (a Phase consistent smoothing routine) and edited again prior to 1D inversions. The 1D inversions allow a quick graphical look at the data in station and profile modes prior to a 2D inversion. Once satisfied that the data were invertible, Invariant (INV), Transverse Magnetic (TM), and Transverse Electric (TE) 2D inversions were calculated, as presented below.

For Lanai, the EDI files were passed onto P. Wannamaker, who ran his proprietary 3D code on the data. Inverted resistivity structure for Lanai is shown in **Fig. 6**.

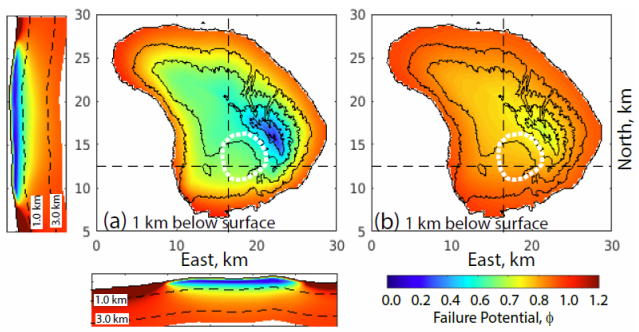

Fig. 4 Failure potential, due to topographic stresses in the crust of Lanai shown at (a) 1 km and (b) 2 km below the surface topography. Vertical cross sections are taken along dashed lines. White dashed oval outlines a median density of 2900 kg/m3 at 3 km depth from gravity inversions (see Fig. 5).

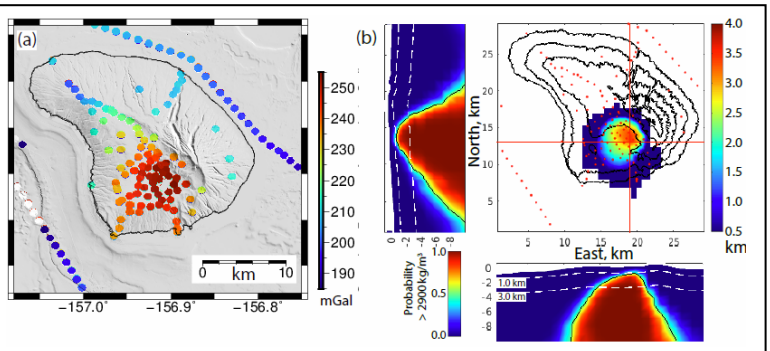

Fig.5 (a) Local complete Bouguer anomaly of Lanai using ρ_0 = 2600 kg/m^3 (colored patches at measurement locations). Topography is illuminated from the NE and the shoreline outlined. (b) Map of the depth below the surface to 90%-probability of densities ≥2900 kg/m3. Subaerial topography is contoured (100 m intervals) and gravity stations are marked with red dots. (c) East-west and (d) vertical cross sections along the lines in (b) showing probability of density >2900 kg/m^3; black contour is for median density of 2900 kg/m^3. Vertical axis is elevation relative to sea level.

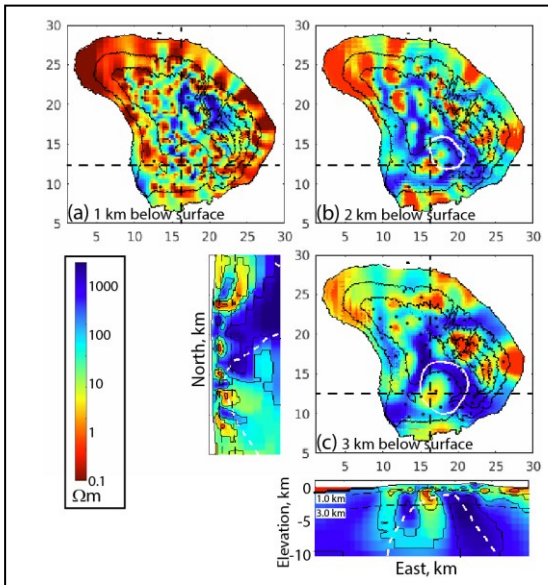

Fig.6 3D resistivity structure from inversions of MT data shown at (a) 1 km, (b) 2 km, and (c) 3 km below the surface. Vertical sections along dashed lines are shown. White curves outline a median density of 2900 kg/m^3 from the gravity inversions.

2.5 Probability Modeling using the Voter-Veto Method

The method developed in PHASE1 for relating geologic, geophysical, and geochemical data to probabilities of a promising geothermal resource centered around two forms of equations (see *Ito et al.* [2016] for details).

2. UPDATED PROBABILITY AND CONFIDENCE MAPS

Our updated statewide assessment incorporates the new data from the water sampling, gravity, MT surveys, as well as calculations of topographic stresses. The new water temperatures, Cl/Mg ratios, SiO_2 data, and the new gravity data were used with geological data to compute the probability of heat following the methodology presented in Ito et al. (2017). Fits of the inverted (3D for Lanai and 2D for Mauna Kea and Maui) resistivity structure to the ideal resistivity profiles were incorporated into calculations of the probability of heat and fluid (Eq. (2)) using the same weighting as in Phase 1. The fit of the computed failure potential to the ideal profiles provided new, additional information about permeability. The numerical values of probability and confidence should (again) be interpreted in a relative (not absolute) sense.

Figures 7 and **8** show the results. The addition of topographic stresses leads to island-wide changes relative to our Phase 1 maps: for probability, the changes are positive or negative and small-amplitude (±0.03 or less), and for confidence the changes were always positive ~ +0.05. Changes over localized areas of more variable amplitude result from the new water and geophysical data. On Kauai

and Oahu, the small-amplitude changes in probability are due mostly to the effects of topographic stresses on the probability of permeability. In Figures 7 and 8, the locations of Phase 2 geophysical work are highlighted in red boxes. Such locations were considered as prospects for Phase 3 drilling. On Lanai, the probability of a resource has been elevated over localized zones due to the MT data, new water temperature measurements, and the failure potential distribution. Confidence in the probability estimates on Lanai increased substantially (> 0.15). At the lower elevations of Haleakala's southwest rift zone (SWRZ) the resource probability is now slightly lower due to the new MT and gravity data, whereas confidence in this area has been elevated to > 0.70.

Around Mauna Kea, probability is little changed along the MT survey lines northwest and east of the summit, whereas the confidence in these areas has increased by 0.05-0.25. South of the summit along Saddle Rd, the probability has increased by 0.05-0.2, whereas the confidence shows little reliable change (the light blue patches are due to revised water data and depend on the precise trajectories of modeled but poorly known groundwater flow). In the central part and southern half of Hawaii Island, resource probabilities are maximal owing to the young ages of the active Mauna Loa and Kilauea volcanoes, which elevate the probability of heat, as well as the ongoing seismic activity and deformation (GPS), which increases the probability of permeability. Probability values for these volcanoes are little changed and confidence remains low over large areas (except near Puna Geothermal Venture leases).

Generally speaking, the probability of heat and fluid can reach high values (>0.8) at coinciding locations on Lanai, Maui, and Mauna Kea Volcano, and so it is the probability of permeability that has the dominant vetoing influence. At these locations the maximal probabilities of permeability are only moderate (0.5-0.6) and thus so are the maximal values of the resource probabilities. This result is reflective of the few data types that inform us about permeability and is consistent with the fact that permeability can vary by several orders of magnitude over short length scales with little or no surface expression. Correspondingly, the probabilities of a viable geothermal resource on SE Mauna Kea and Lanai are limited mostly by our knowledge of permeability. For reference, the probabilities at these two areas (considered targets for drilling) are about 50% of the probability computed for the PGV geothermal power plant, largely due to their lower probability of permeability; around PGV, a higher probability of permeability is predicted from the more active seismicity and deformation in that area.

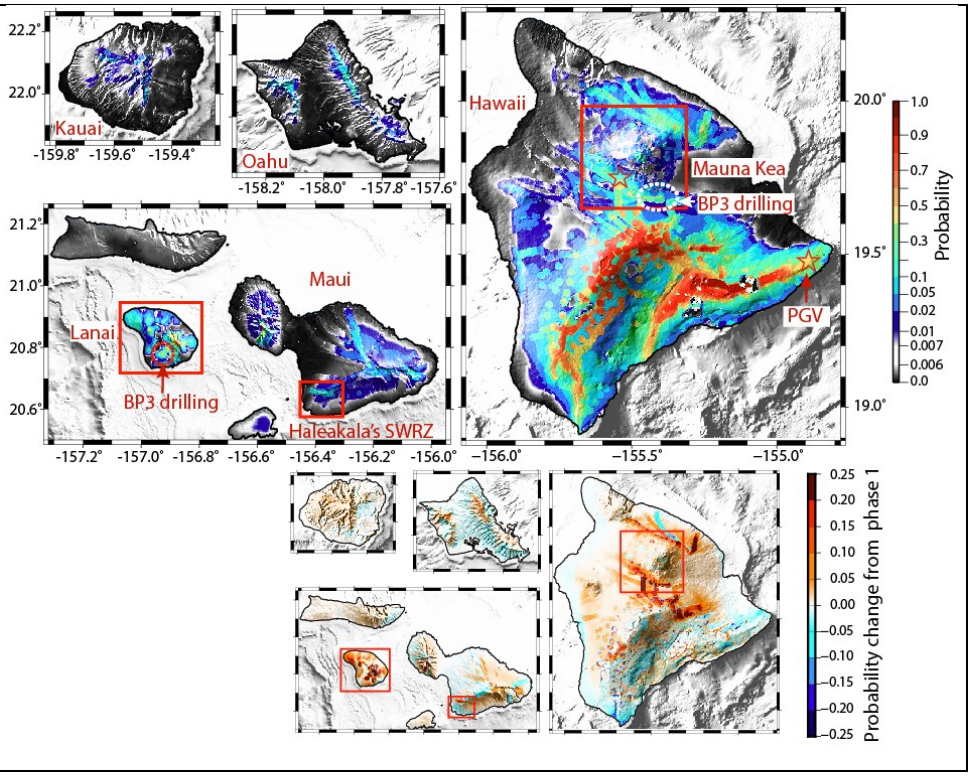

Fig. 7 New resource probability maps. Red boxes outline areas of Phase 2 focused geophysical surveying. Stars indicate the Saddle Drill site (north) where high-temperatures were found, and Hawaii's one geothermal production site, Puna Geothermal Ventures (PGV). Changes in probability relative to the Phase 1 assessment are shown below (warm colors show increased probability).

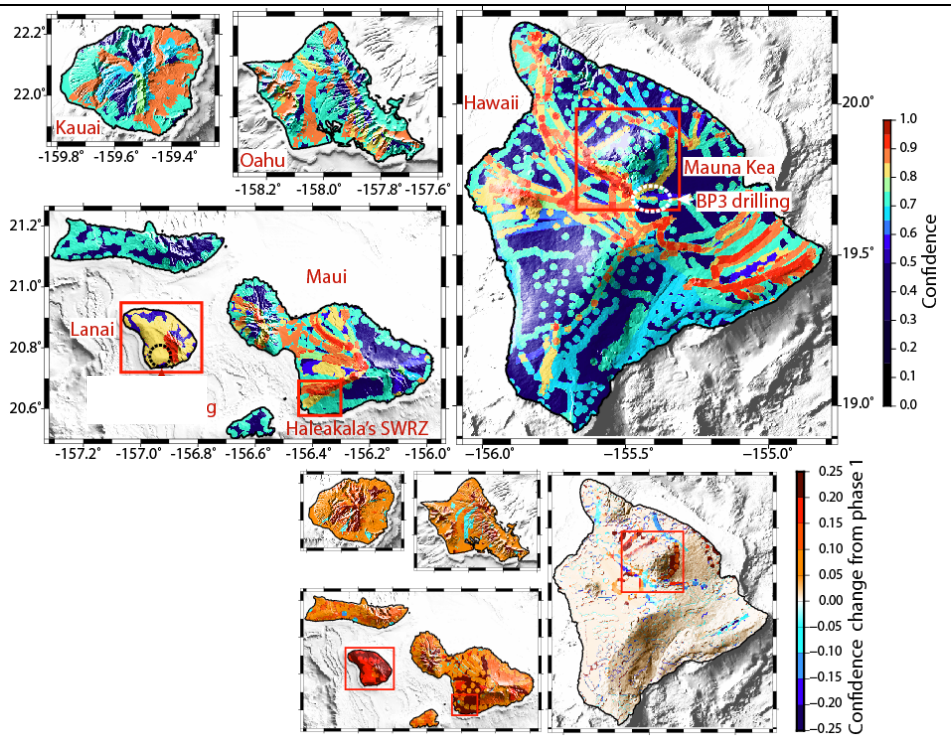

Fig. 8 New maps of confidence in the probabilities. Changes in confidence relative to the Phase 1 assessment are shown below (warm colors show increased confidence)

2. SUMMARY AND CONCLUSIONS

Phase 2 of the Hawaii Play Fairway project involved the collection of new groundwater data in 10 areas from Kauai to Hawaii Island, and the collection of magnetotelluric and gravity data on Lanai, Haleakala Volcano's SW rift zone (Maui), and central Hawaii Island. We also modeled topographically induced stress in order to better characterize subsurface permeability. Finally all data were incorporated into updated resource probability maps for the State of Hawaii. Locations where geophysical surveys were performed are considered prospects for drilling. Inversion geophysical data for Lanai and SSE Mauna Kea revealed high gravity (interpreted to be dikes) and conductive regions (interpreted to be warm fluid) at a depth of 1.5 to 2 km, and as such were our top drilling targets. The same data from the Haleakala SW rift and E of Mauna Kea showed promising resistivity, but were not coincident with high gravity.

REFERENCES

GRAV3D, 2015. A program library for forward modeling and inversion of gravity data over 3D structures, in: Joint/Cooperative Inversion of Geophysical Data, Ver. 5.0, UBC Geophysical Inversion Facility, Univ. British Columbia, Vancouver

Ito G., Frazer N., Lautze N., Thomas D., Hinz N., Waller D., Whittier R., Wallin, E. 2017, Play Fairway Analysis of Geothermal Resources across the State of Hawaii: 2. Resource Probability Mapping, Geothermics 70: 393-405

Lautze N., Thomas D., Hinz N., Apuzen-Ito G., Frazer N., Waller D. 2017a, Play Fairway Analysis of Geothermal Resources across the State of Hawaii: 1. Geological, geophysical, and geochemical datasets, Geothermics 70: 376-392

Lautze N., Thomas D., Waller D., Hinz N., Frazer N., Apuzen-Ito G., 2017b, Play Fairway Analysis of Geothermal Resources across the State of Hawaii: 3. Use of Development Viability as one criteria to prioritize future exploration activities. Geothermics 70: 406-413

Lautze N., Apuzen-Ito G., Thomas D., Tachera, D., Martel, S., Hinz N., Frazer N., Whittier, R. in prep, Play Fairway Analysis of Geothermal Resources across the State of Hawaii: 4. Improving the Statewide Resource Assessment through collection of groundwater and geophysical data and stress modeling

Love, A.E.H., 1929. The stress produced in a semi-infinite solid by pressure on part of the boundary, Philosophical Transactions of the Royal Society of London, series A, v. 667, p. 377– 420

Martel, S.J., 2000, Modeling elastic stresses in long ridges with the displacement discontinuity method: Pure and Applied. Geophysics: special issue on landslides and tsunamis, v. 157, p. 1039-1057

Martel, S.J., 2016, Effects of small-amplitude periodic topography on combined stresses due to gravity and tectonics: International Journal of Rock Mechanics & Mining Sciences, v. 89, p. 1-13

Martin, T. Carol D., Brockhoff A., Creed J. Stephen, Long E. (1992), Determination of metals and trace elements in water and wastes by inductively coupled plasma-atomic emission spectrometry. Methods for determination of metals in environmental samples. CRC Press Inc., Boca Raton, 33-91

Moore, J.G. (2001). Density of basalt core from Hilo drill hole, Hawaii, J. Volc. Geotherm. Res., 112, 221-230

Pfaff, J. D., D. P. Hautman, D. J. Munch (1993), Determination of Inorganic Anions in Drinking Water by Ion Chromatography EPA Method 300

Torres, Marta E., A.C. Mix, and W.D. Rugh (2005), "Precise δ13C analysis of dissolved inorganic carbon in natural waters using automated headspace sampling and continuous-flow mass spectrometry." Limnol. Oceanogr.: Methods 3, 349-360